



Short communication

Investigation of oxygen exchange kinetics in proton-conducting ceramic fuel cells: Effect of electronic leakage current using symmetric cells



Daniel Poetzsch, Rotraut Merkle*, Joachim Maier

Max Planck Institute for Solid State Research, Heisenbergstrasse 1, 70569 Stuttgart, Germany

H I G H L I G H T S

- Effect of minority hole-conductivity in BaZrO₃ on impedance analysis of electrode reaction.
- Electronic leakage current dominates impedance spectra on pore-free electrodes.
- Approaches to exclude or diminish the leakage current, or to correct the impedance spectra are shown.

A R T I C L E I N F O

Article history:

Received 22 December 2012

Received in revised form

8 April 2013

Accepted 23 May 2013

Available online 5 June 2013

Keywords:

H⁺-SOFC

Oxygen reduction mechanism

BaZrO₃ electrolyte

Hole conductivity

A B S T R A C T

Pore-free microelectrodes (20–100 μm diameter, 100 nm thick) of mixed-conducting perovskites are prepared on dense pellets of Y-doped BaZrO₃ (4–15% Y) as proton-conducting electrolyte. The oxygen reduction reaction is investigated in gas-symmetric cells using AC impedance spectroscopy. The electronic resistance owing to the non-negligible hole conductivity of acceptor-doped BaZrO₃ in oxidizing atmosphere can – even though much larger than the ionic resistance – be much lower than the resistance of the oxygen exchange reaction. This results in a substantial impact of electronic leakage current on the impedance spectroscopic investigations of the oxygen reduction process. Solutions to this problem are demonstrated. The impact of this effect for porous electrodes is discussed.

© 2013 Elsevier B.V. All rights reserved.

1. Introduction

Solid oxide fuel cells using proton (H⁺-SOFC) instead of oxide conducting electrolytes (O²⁻-SOFC) have the potential of reducing the operating temperature from ~800 °C to an intermediate temperature regime of 400–700 °C. A further advantage is the formation of water at the cathode, i.e. the fuel is not diluted. Nevertheless, the oxygen reduction at the cathode remains the main limiting feature of such a fuel cell, and a detailed understanding of the reaction mechanism – which probably differs from that for O²⁻-SOFC – has not been achieved yet. The increased interest in this topic is reflected in several publications (see e.g. [1] (Pt electrodes) [2–5], (mixed-conducting perovskites)); in which, however, porous electrodes have been used. While the overall performance of such cells can be evaluated, it is difficult to extract

reliable mechanistic information, as the electrode morphology is complex, and varying with preparation details and materials composition. In contrast, dense thin films provide the possibility to investigate the oxygen reduction mechanism under well-defined conditions, and are used in the present study combined with an extended, reversible counter electrode [6–8].

Water-containing Y-doped BaZrO₃ combines high bulk proton conductivity with excellent chemical stability [9–11]. Space charge depletion zones have been identified as the main origin of the drastically decreased proton conductivity at the grain boundaries [12–14] and can be mitigated by a high dopant content and suitable processing (see e.g. [15–17]). Such acceptor-doped perovskites (zirconates, cerates) exhibit also some minor conductivity contributions by electrons (holes) and oxide ions (vacancies) [18,19]. The actual magnitude depends on oxygen and water partial pressures (*p*O₂, *p*H₂O) and temperature. The electronic transference number *t*_{eon} can reach up to 0.2 in humidified O₂ (in dry O₂ even more) [19].

In the present study we will show that for measurements on gas-symmetric cells (same gas at both electrodes) in high *p*O₂ the

* Corresponding author. Tel.: +49 711 6891768; fax: +49 711 6891722.
E-mail address: r.merkle@fkf.mpg.de (R. Merkle).

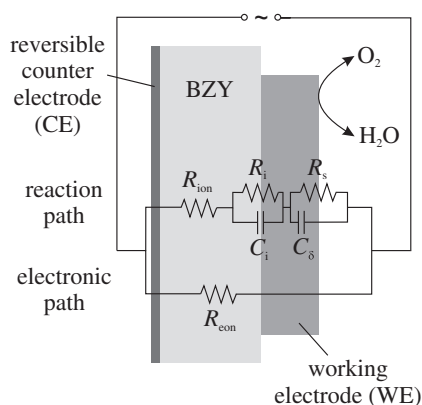


Fig. 1. Electrochemical cell for investigating oxygen kinetics on proton-conducting oxides and its equivalent circuit. For microelectrodes, the extended counter electrode (CE) can be considered reversible due to its much larger size [7]. The “short-circuiting” of the Faradaic current (“reaction path” through R_{ion} , R_i and R_s) by the “electronic leakage path” R_{eon} becomes significant if the surface exchange reaction is kinetically impeded as shown here.

minor electronic contribution drastically affects the apparent electrode resistance caused by the oxygen exchange surface reaction. This important aspect – with substantial consequences also on the mechanistic interpretation – has not been discussed in the literature. Only Lai and Haile [20,21] discussed the effects of Samarium doped CeO_2 (SDC) becoming a mixed ionic–electronic conductor at low $p\text{O}_2$ (with electronic transference number up to 0.75) using porous Pt or BSCF electrodes; however, the electrode response is a side aspect in their study.

Notwithstanding the fact that the influence of a non-negligible electronic transference number is usually more severe for pore-free electrodes, the effect can also be significant for porous electrodes. In a real fuel cell with hydrogen at the anode this problem is absent because the gradient of the oxygen chemical potential across the electrolyte will lead to formation of a region where t_{eon} approaches zero. Thus, this discussion, even though questioning the validity of some previous kinetic studies on proton conductors, does *not* raise doubts on the applicability of perovskite proton conductors for H^+ -SOFC.

2. Setting out the problem

For proton-conducting perovskites, oxygen vacancies $\text{V}_\text{O}^{\bullet\bullet}$ are introduced by acceptor-doping and can be hydrated forming protonic defects $\text{OH}_\text{O}^\bullet$, eq. (1). However, incorporation of oxygen (eq. (2)) competes with the water uptake by introducing electron holes h^\bullet affecting the electronic conductivity.



All these carrier concentrations depend on acceptor content, temperature, $p\text{O}_2$ and $p\text{H}_2\text{O}$. Below 600 °C protonic defects are the dominant species in wet atmosphere, and according to their high mobility compared to oxygen vacancies they contribute most to the total conductivity (transference number t_{ion} of ~ 0.9 [18,19]). With increasing T and decreasing $p\text{H}_2\text{O}$ (dehydration) and increasing $p\text{O}_2$ (shifting reaction (2) to the right) the hole concentration increases, being, nevertheless, lower than the proton concentration. However, due to their very high mobility the holes can reach perceptible transference numbers from 0.05 to 0.2 [19]. In contrast, Y stabilized

zirconia (YSZ) as oxide conducting electrolyte has a negligible electronic transference number $t_{eon} < 10^{-7}$ [22].

For the investigation of oxygen exchange kinetics gas-symmetric cells are frequently used in which the whole setup is under oxidizing atmosphere ($t_{eon} \approx 0.05$ – 0.2). We will first focus on the case of pore-free (micro-)electrodes. Fig. 1 shows the equivalent circuit for this situation. The “reaction path” describes the electrochemical reduction of oxygen (Faradaic current) followed by ionic carrier migration through the electrolyte.

Compared to the very general model by Jamnik and Maier [23] used also by Lai and Haile [20,21] for Pt|SDC|Pt, the present circuit for perovskite electrodes on BZY omits the “transmission line” connecting the ionic (R_{ion}) and electronic rails (R_{eon}) with chemical capacitors. This can be justified by the following considerations. Owing to the small thickness of a typical dense (micro-)electrode (100 nm) a very small protonic conductivity in BSCF suffices to enable the “bulk path”¹ for the surface exchange reaction (oxygen reduction to H_2O). Such a situation, with the surface reaction resistance largely limiting the oxygen reduction rate in the “bulk path”, leads to the appearance of a large chemical capacitance C_δ in the electrode response ($>1000 \text{ F cm}^{-3}$ as extracted from the impedance spectra, related to the whole active volume of the electrode material). This chemical capacitance is much larger compared to a Pt|SDC interface where the reaction proceeds only via the triple phase boundaries with a low C_δ . Furthermore, BZY is supposed to have a low chemical capacitance ($<10 \text{ F cm}^{-3}$),² in contrast to SDC at low $p\text{O}_2$ (ca. 300–1000 F cm^{-3} [20,21]). Consequently, the chemical capacitance in BZY is small compared to BSCF and thus, the capacitors contacting the ionic and electronic rail can be neglected. The Jamnik–Maier model simplifies to the circuit shown in Fig. 1.

The ionic resistance R_{ion} in the electrolyte is inversely proportional to σ_{ion} ; for microelectrodes with diameter d the proportionality factor is $1/2d$ [26]. In the following, R_{ion} (and R_{eon}) comprises bulk and grain boundary contributions of the polycrystalline electrolyte; the respective capacitances are neglected as for microelectrodes they are in the range of the stray capacitance. The ion transfer from the electrolyte to the electrode may lead to a semicircle at intermediate frequencies with resistance R_i and double-layer capacitance C_i . The surface exchange reaction (oxygen reduction to H_2O) gives rise to a resistance R_s ($R_s \propto (k^q)^{-1}$ with k^q = effective rate constant; “surface reaction resistance”) in parallel to a chemical capacitance C_δ which refers to the whole volume of the mixed-conducting electrode material. Owing to the smaller actual surface area, R_s for pore-free (micro-)electrodes is much larger than for extended, porous electrodes. Its dependence on T , $p\text{O}_2$, $p\text{H}_2\text{O}$ and microelectrode geometry gives important pieces of information about the rate determining step. The “electronic path” (non-faradaic current, no contribution from oxygen reduction reaction) is parallel to the reaction path and is created by the electronic (hole) conductivity in the electrolyte, associated with a finite resistance R_{eon} . Using AC impedance spectroscopy the three

¹ For (La,Sr)MnO_{3±δ} at 800 °C an ionic conductivity of $3 \times 10^{-8} \text{ S cm}^{-1}$ is enough to enable the “bulk path” in which the oxide ions being involved in the surface exchange reaction are transported through the bulk of the electrode material and the reaction is not limited to the triple phase boundary only [6]. Assuming a similar proton diffusion coefficient in BSCF as in BZY ($10^{-5} \text{ cm}^2 \text{ s}^{-1}$ at 800 °C [24]) already a proton concentration as small as 10^{-7} mol\% in BSCF would yield a sufficient conductivity for protons to migrate from BZY through the BSCF electrode to the BSCF/gas surface. Furthermore, the measured dependence of R_s for dense BSCF electrodes on BZY4 rather scaling with the microelectrode area than the circumference (cf. Table 1) supports that the oxygen reduction occurs by the bulk path.

² Oishi et al. [25] give the proton concentration in 10% Y-doped BaCeO₃ at different oxygen partial pressures. The concentration does not perceptibly change, corresponding to a low chemical capacitance. BZY is expected to behave similarly.

contributions in the reaction path can be resolved. At high frequencies (HF) C_i and C_δ are permeable and the parallel combination of R_{ion} and R_{eon} is measured. In the middle frequency range (MF) C_i is blocking and the parallel combination of $(R_{ion} + R_i)$ and R_{eon} is obtained. In the low frequency (LF) or DC range C_i and C_δ are blocking and the parallel combination of $(R_{ion} + R_i + R_s)$ and R_{eon} is measured. Thus, the measured resistance approaching zero frequency represents only an upper bound to $(R_{ion} + R_i + R_s)$. The severeness of the “electronic short-circuit” depends on the relative magnitude of $(R_{ion} + R_i + R_s)$ and R_{eon} .

Based on literature data the relations between the resistances can be quantified as: $R_{ion} \approx 0.05–0.25R_{eon}$ ($t_{eon} = 0.05–0.2$) [18,19], $R_{ion} \approx R_i$ and $R_s \gg R_{ion}$ (perovskite microelectrodes on YSZ, [7,8,27]). In Fig. 2 impedance spectra are simulated based on the equivalent circuit in Fig. 1 using Zview 3.3a (Scribner Associates, Inc.) and typical values (i) without ($R_{eon} = \infty$, top) and (ii) with R_{eon} in parallel (bottom). The spectrum without R_{eon} consists of a HF intercept (R_{ion}), MF ($R_i C_i$) and LF semicircle ($R_s C_\delta$). Allowing for an “electronic short-circuit” with $R_{eon} = 8R_{ion}$ ($t_{eon} = 0.1$) the measured surface reaction resistance R_s (respectively, R'_s ,³ diameter of LF semicircle) decreases by one order of magnitude from 7 to $0.6 \Omega \text{ cm}^2$, and R'_i appears more prominent.⁴ The simple reason is that for pore-free electrodes R_s is up to orders of magnitude larger than R_{eon} ; hence, the measured impedance is dominated by the short-circuiting by R_{eon} . This prediction will be supported by experimental results in Section 4, and implications for porous electrodes discussed in Section 5.

3. Experimental part

Powders of $\text{Ba}(\text{Zr,Y})\text{O}_{3-\delta}$ (BZY) with 4, 6 and 15% Y were synthesized by solid state reaction from BaCO_3 (99%, Alfa Aesar, USA) and $(\text{Zr,Y})\text{O}_{2-\delta}$ (YSZ, Tosoh TZ-0Y, TZ-3Y and TZ-8Y, Japan). Dense pellets ($\sim 99\%$) obtained by spark plasma sintering at 1600°C and 50 MPa pressure for ~ 5 min (heating with ~ 0.6 to ~ 1.4 kA DC current without pulse sequence) and post-annealing for 20 h at 1700°C in air [17] were cut into $5 \times 5 \times 0.5$ mm substrates and fine-polished. 100 nm thin, pore-free films of $\text{Ba}_{0.5}\text{Sr}_{0.5}\text{Co}_{0.8}\text{Fe}_{0.2}\text{O}_{3-\delta}$ (BSCF) were applied by pulse laser deposition (PLD) and patterned into circular microelectrodes by photolithography. The half-cell of BSCF microelectrodes on BZY electrolyte was glued on a sapphire plate with silver paste (Demetron, Germany) and silver foil, forming the porous counter electrode (for details see Ref. [8]). The microelectrodes (=working electrode) were contacted by PtIr needles (Moser Jewel Company, USA). Impedance spectra were recorded using an Alpha High Resolution Dielectric Analyser with a POT/GAL 15V 10A Electrochemical Impedance Test Interface (Novocontrol, Germany) (20 mV AC amplitude, 10^6 to 10^{-2} Hz frequency) between 350 and 700°C , 10^{-4} to 1 bar $p\text{O}_2$, 0.2–20 mbar $p\text{H}_2\text{O}$ and 20–100 μm microelectrode diameter.

4. Results

Typical impedance spectra for BSCF cathodes on YSZ and BZY are shown in Fig. 3a and b. Strong differences appear especially for the LF arc. The spectrum for BZY exhibits a small contribution at intermediate frequencies ($R_i = 24 \text{ m}\Omega \text{ cm}^2$, $C_i = 1 \text{ mF cm}^{-2}$; C_i being in the range of double-layer capacitances) attributed to carrier

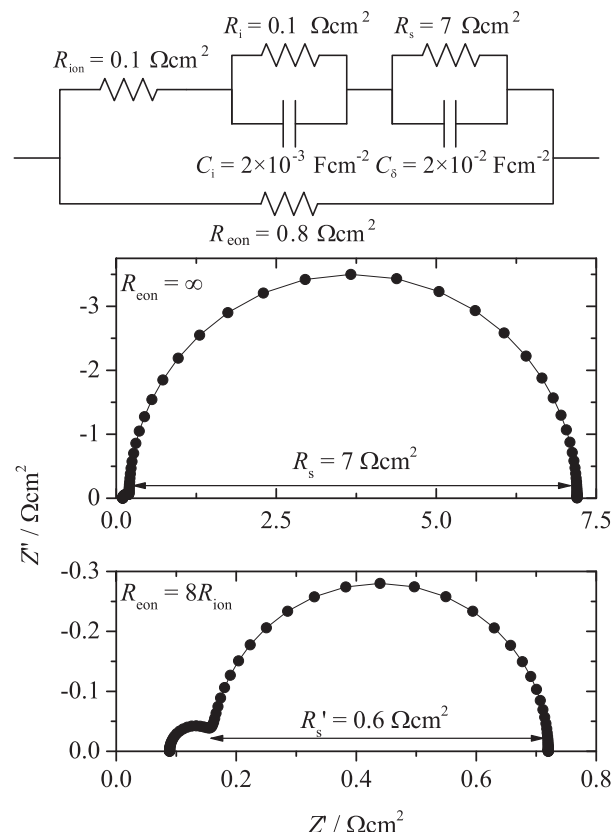


Fig. 2. Simulated impedance spectra based on the given equivalent circuit. The values are chosen to be close to those measured on microelectrodes. The resistances and capacitances are normalized to a $60 \mu\text{m}$ microelectrode. C_δ normalized to the volume of a 100 nm thick microelectrode is $\sim 2000 \text{ F cm}^{-3}$.

transfer at the electrode/electrolyte interface. The low-frequency semicircle has a large capacitance of about 25 mF cm^{-2} , clearly higher than for a double layer. The resistance R'_s of the LF semicircle on BZY is two orders of magnitude lower than on YSZ. Although oxygen exchange might be faster on a proton conductor (where oxygen reduction does not necessarily involve oxygen incorporation), this is not expected to amount to several orders of magnitude.

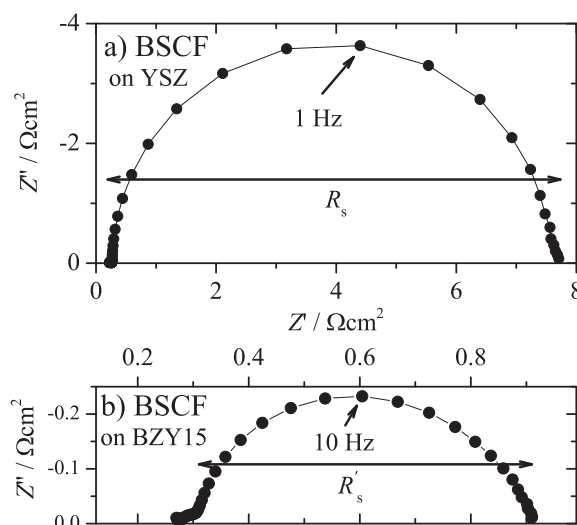


Fig. 3. Typical impedance spectra of a pore-free BSCF $60 \mu\text{m}$ microelectrode on a) YSZ (750°C , 1100 ppm O_2 , dry) and b) BZY15 (700°C , 1100 ppm O_2 , humid).

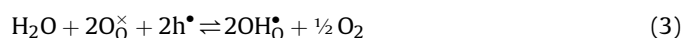
³ Resistance values influenced by R_{eon} will be called “apparent” resistances and denoted with a $'$.

⁴ All three resistances of the reaction path are disturbed by R_{eon} . As this influence is most pronounced for R_s , and as R_s contains most mechanistic information for oxygen exchange kinetics, R'_{ion} and R'_i are excluded in the discussion.

Hence, the measured, apparent R'_s on BZY is most probably not the real one. On the other hand, there are strong similarities with Fig. 2: The spectra simulated with $R_{\text{eon}} = \infty$ and measured on YSZ, and simulated with $R_{\text{eon}} = 8R_{\text{ion}}$ and measured on BZY, respectively, exhibit the same characteristics. The electronic conductivity in YSZ is approximately five orders of magnitude lower than in BZY [22]; consequently, the measured spectrum on YSZ looks like the simulation with an infinite R_{eon} . For BZY the simulation result suggests that the low apparent R'_s is caused by the low R_{eon} as described in Section 2.

The dependency parameters for R_s and R'_s are summarized in Table 1. All dependencies are smaller for BSCF on BZY than on YSZ, and do not provide a consistent mechanistic picture. The lower activation energy and $p\text{O}_2$ dependence could possibly be explained by a different mechanism and/or rate determining step. In contrast, the $p\text{H}_2\text{O}$ dependence is counter-intuitive as a better kinetic performance is expected in wet atmosphere considering protonic defects as the main carrier. The most questionable result is the apparent diameter dependence as it is neither water formation at triple phase boundary (linear dependence with -1) nor on the whole surface area (square dependence with -2).

On the other hand these results can well be understood considering that R'_s results from the parallel combination of R_s and R_{eon} . Therefore, combined dependencies are measured, which is most obvious for the diameter and $p\text{H}_2\text{O}$ dependence. The measured values (1.4–1.8) lie in between -1 (value for R_{eon} defined as spreading resistance [26]) and -2 (value for bulk path of R_s). R_s decreases with water partial pressure, R_{eon} increases as holes are destroyed according to eq. (3) (cf. experimental data in Ref. [19]). As the measured impedance is essentially determined by R_{eon} , R'_s increases as well. Furthermore, on decreasing the dopant concentration from 15 to 4% Y (increasing R_{eon}) the diameter dependency approaches -2 (characteristic for bulk path) and the $p\text{O}_2$ dependence increases to values above 0.5 (often found for the oxygen reduction reaction on perovskites); indicating that R'_s is getting closer to R_s .



A hypothetical explanation for the “intermediate” dependencies could be that under the present measurement conditions by chance bulk and triple phase boundary path contribute comparably. While this could explain the diameter dependence, and agrees with the temperature and $p\text{O}_2$ dependence, it hardly explains the $p\text{H}_2\text{O}$ dependence and low overall impedance. Furthermore, one would expect dominance of either bulk or triple phase boundary path under certain conditions. Although an extended T and $p\text{O}_2$ range is studied a change in the mechanism is not observed. Finally, the minimum concentration of protons in the electrode material required for enabling the bulk path is estimated to only $\sim 10^{-7}$ mol % (see footnote 1). With this very low concentration and the surface area being much larger than the active area close to the triple-phase-boundary, the bulk path has to be dominant at lower T and

higher $p\text{H}_2\text{O}$ (higher proton concentration in the electrode). Thus, the hypothesis of mixed bulk and triple phase boundary path cannot explain all experimental results; in contrast, taking R_{eon} into account, all observations can be understood qualitatively and, in principle, also quantitatively.

Last but not least, the strongest evidence is the fact that the measured R'_s for BSCF films deposited under identical conditions depends on the electrolyte (cf. Fig. 5, see discussion in Section 6). Although R_{ion} and R_s are well separated in the impedance spectra, there must be a coupling between the measured surface reaction resistance and the electrolyte properties which is only provided by the electronic leakage current (R_{eon} in electrolyte).

5. Consequences for porous electrodes

Whether or not the described problem is relevant for the frequently used porous electrode systems is discussed now. On dense electrodes the problem originates from the fact that R_s can be orders of magnitude larger than R_{eon} . On porous electrodes the real surface area is three to seven orders of magnitude larger than the area of a dense (micro)electrode,⁵ resulting in the absolute R_s being orders of magnitude lower. Hence, the ratio between R_s on porous electrodes and R_{eon} is lower and the effect of R_{eon} is much less pronounced. For quantification typical values are used; electrode particle size of $\sim 1 \mu\text{m}$, electrode layer thickness of $\sim 10 \mu\text{m}$, 50% porosity, and $\sim 10 \mu\text{m}$ thick electrolyte. Assuming a similar area specific resistance as for dense microelectrodes, R_s on porous electrodes (calculated with the large, real surface area) and R_{eon} lie in the same order of magnitude. The ratio R'_s/R_s is calculated for given R_{ion} , R_{eon} and R_s according to equ. (4)⁶

$$\frac{R'_s}{R_s} = \frac{R_{\text{eon}}^2}{(R_{\text{ion}} + R_{\text{eon}} + R_s) \times (R_{\text{ion}} + R_{\text{eon}})} \quad (4)$$

and shown in Fig. 4. The ratio of R_{ion} and R_{eon} is fixed here to $R_{\text{ion}} = 0.1R_{\text{eon}}$ ($t_{\text{eon}} = 0.09$ is an average value for BZY) because usually R_{ion} and R_{eon} cannot be varied independently (proton and hole concentration both depend on acceptor concentration). In the deep red area R_{eon} is much larger than R_s , hence, R_{eon} hardly influences R'_s and R'_s/R_s is close to unity (the fact that it does not reach exactly unity is discussed in the next section). The deep blue part shows the typical situation for pore-free electrode measurements. R_s is much larger than R_{eon} which becomes dominant, and R'_s/R_s is close to zero.

When R_s and R_{eon} are of the same order of magnitude (typical for porous electrodes), the ratio R'_s/R_s is very sensitive to changes in R_{eon} or R_s . This is illustrated in Fig. 4 by two exemplary situations: (i) Comparing electrode materials with the same R_s values (same catalytic activity) on electrolyte substrates with different R_{eon} (different materials or preparation route) – points A and B in Fig. 4. Although the R_s values are the same, the measured, apparent R'_s differ significantly, and are too low. (ii) Comparing electrode materials with different R_s values (different materials or morphology) on substrates with the same R_{eon} – points A and C. Again, the absolute, measured R'_s values are too small, and the relative difference between both measurements is underestimated. Consequently, not considering that R_{eon} causes these differences, significantly wrong

Table 1

Measured activation energies E_a , diameter d dependence x and partial pressure dependencies of oxygen (n) and water (m) of the electronic resistance in BZY $R_{\text{eon,BZY}}$ and the LF resistances for BSCF $R'_{s,\text{BSCF}}$ on BZY and $R_{s,\text{BSCF}}$ on YSZ [8]. The range given for $R'_{s,\text{BSCF}}$ covers the results from BZY15 to BZY4.

Characteristic kinetic parameters	$R_{\text{eon,BZY}}$	$R'_{s,\text{BSCF}}$ on BZY	$R_{s,\text{BSCF}}$ on YSZ
Temperature dep.: E_a in $R \propto e^{-E_a/kT}$	~ 1 eV	1.2–1.5 eV	1.6 eV
Diameter dep.: x in $R \propto d^{-x}$	1	1.4–1.8	2
$p\text{O}_2$ dep.: n in $R \propto p_{\text{O}_2}^{-n}$	1/4	0.4–0.6	0.73
$p\text{H}_2\text{O}$ dep.: m in $R \propto p_{\text{H}_2\text{O}}^{-m}$	$-1/2$	<0	$>0^a$

^a The $p\text{H}_2\text{O}$ dependence was not measured for BSCF but for LSCF [30]; nevertheless, BSCF is expected to behave similarly.

⁵ The relation of the surface areas and of R_s to R_{eon} strongly depends on the microstructure of the electrode layer.

⁶ The interface resistance R_i is neglected in the discussion. As its value can be in the same order of magnitude as R_s for porous electrodes, it modifies the quantitative results; however, it would only complicate the discussion but not change the qualitative statement.

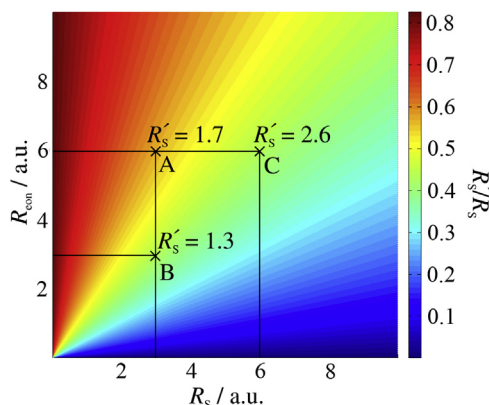


Fig. 4. Ratio R'_s/R_s between the measured, apparent resistance R'_s (parallel combination of R_s and R_{eon}) and the real electrode resistance R_s as function of R_s and R_{eon} . R_s and R_{eon} are chosen to be in the same order of magnitude. Two exemplary cases are illustrated in the plot (A, B, C) – see text.

conclusions might be drawn. Since the exact morphology of porous electrodes is hard to reproduce and also R_{eon} might vary to some degree (in particular for BZY, see e.g. [28]) one has to be very careful with absolute R_s values. This might also be the reason why some mechanistic results in the literature apparently contradict each other. Taking R_{eon} into account, though, may help to explain such puzzling observations.

6. Approaches to solving the problem

Having recognized the problem, four different solution approaches can be suggested.

- (i) Decreasing the acceptor-dopant concentration in the electrolyte, which increases R_{eon} and R_{ion} simultaneously (t_{eon} is typically left unchanged, which is the reason why R'_s/R_s in Fig. 4 never reaches unity). Fig. 5 (inset) shows measured impedance spectra of BSCF microelectrodes on BZY15, BZY6 and BZY4 electrolytes. The measured oxygen reduction

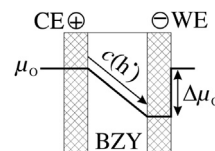


Fig. 6. Profile of oxygen chemical potential under cathodic bias at the WE. As the CE is reversible μ_{O} does not change there. For details see Ref. [31].

resistance R'_s (low frequency semicircle) increases with decreasing Y-content because R_{eon} increases (whereas R_s is assumed to remain unchanged). Consequently, the measured impedance R'_s is closer to R_s on BZY4 than on BZY15. Nevertheless, R_{eon} is still in the order of R_s (see point iv), i.e. $R'_s < R_s$; hence, further decreasing of the dopant concentration would be necessary. Unfortunately, in the limit of an undoped electrolyte R_{ion} will dominate the overall impedance not allowing distinguishing R_s in the spectra anymore. Hence, this approach alone is not sufficient, in particular for pore-free electrodes (large R_s).

- (ii) Inserting an additional layer between BZY and the counter electrode which blocks the electronic current but is permeable for the protons; hence, R_{ion} is not (or less) affected which is the main difference to approach (i). To the best of our knowledge, no proton-conducting acceptor-doped oxide suitable for high T exists so far. Therefore, a layer of proton-conducting potassium hydroxide (melting point 406 °C) was used. Fig. 5 shows that the LF semicircle increases by a factor of five between BZY6 electrolyte without and with KOH-layer, which could be close to the real R_s value. Nevertheless, operating with molten KOH requires further improvements in the experimental setup.
- (iii) Strongly decreasing the hole concentration in the electrolyte (BZY) by introducing a large gradient in the chemical potential of oxygen μ_{O} across the electrolyte. This occurs in a fuel cell configuration exposing the CE (anode) to reducing atmosphere. For microcontacts this is experimentally difficult. A much easier method is measuring with an applied cathodic DC bias, such that the chemical potential of oxygen μ_{O} at the micro-WE is reduced by orders of magnitude (a bias of 200 mV corresponds to $\log(p_{\text{O}_2}/p_0) = 5.2$ at 500 °C according to Nernst's Equation). Therefore, the hole concentration in BZY would decrease from CE to WE (cf. Fig. 6). According to a comparison with p_{O_2} dependent conductivity measurements in BZY from Nomura and Kageyama [18], at 200 mV bias ($\log(p_{\text{O}_2}/p_0) \approx 5$) the purely ion-conducting regime is reached. An electronically blocking layer forms in the electrolyte and the leakage current is suppressed. R_{eon} increases, and R_s decreases⁷ under cathodic bias, shifting R'_s to the R_s -dominated regime. Fig. 5 shows that the expected tendency is clearly visible; with increasing R_{eon} the measured R'_s increases and comes closer to the real value of R_s (which is still unknown).
- (iv) Precise quantification of R_{eon} to correct R'_s for the “electronic leakage”. For $R_{\text{eon}} \ll R_s$ (BZY15 and BZY6) this does not work as even a small error of 5–10% for R_{eon} leads to a large error for R_s . For conditions where $R_{\text{eon}} \approx R_s$ or $R_{\text{eon}} > R_s$ (BZY4, or porous electrodes with a larger area active for oxygen reduction) it works; however, the quantitative analysis requires still great

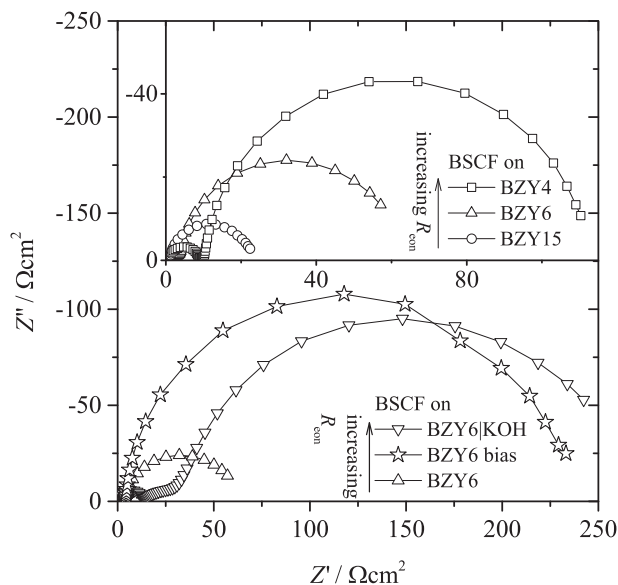


Fig. 5. Measured impedance spectra of BSCF 60 μm microelectrodes on different proton-conducting electrolytes at 500 °C, 1000 ppm O_2 and 20 mbar pH_2O . The BZY6 bias spectrum was measured under 200 mV cathodic DC voltage.

⁷ The real R_s on BZY behaves similarly as for BSCF on YSZ, i.e. decreases with cathodic as well as anodic bias ([7,8], see Ref. [29] for the more complex quantitative interpretation).

care. On microelectrodes R_{eon} can easily be measured by using a dense gold layer as microelectrode to block the reaction path; then R_{eon} is measured as DC resistance [32].

7. Conclusions

Electrochemical impedance data of the oxygen reduction reaction measured in gas-symmetric cells have to be analyzed with care when the electrolyte's electronic resistance is comparable to or smaller than the electrode's surface reaction resistance. This problem arises in particular for acceptor-doped, proton-conducting perovskite electrolytes which typically exhibit $t_{\text{eon}} \approx 0.05$ – 0.2 under oxidizing atmosphere. Such conditions provide a non-faradaic leakage path. Since the impedance of the surface reaction is comparatively high on dense electrodes (low surface area), the overall impedance is sensitive with respect to an electronic short-cut, even if the electronic conductivity in BZY is small compared with the ionic one. In the worst case, the total impedance would be, in spite of a possibly low electronic transference number, dominated by the leakage path; making the extraction of the reaction kinetic parameters impossible (temperature, partial pressure and diameter dependence). Even on porous electrodes the impedances of both pathways (electronic transport path and reaction path, see Fig. 1) can be of similar magnitude; and the electronic conductivity in the electrolyte has to be taken into account for a reliable analysis.

Moreover, we pointed out four possible solutions to decrease or even exclude the influence of this leakage path. A detailed quantitative discussion for BZY, focussing in particular on the oxygen reduction mechanism is beyond the scope of the present paper and will be given elsewhere.

Acknowledgement

The authors thank Y. Link, B. Stuhlhofer and S. Schmid for gold deposition, PLD and Photolithography (Technology Service Group), G. Götz for XRD and the Crystal Preparation Group (all at the Max Planck Institute for Solid State Research, Stuttgart, Germany).

References

- [1] H. Uchida, S. Tanaka, H. Iwahara, *J. Appl. Electrochem.* 15 (1985) 93–97.
- [2] B. Wei, Z. Lu, X.Q. Huang, M.L. Liu, N. Li, W.H. Su, *J. Power Sources* 176 (2008) 1–8.
- [3] Y. Lin, R. Ran, Y. Zheng, Z.P. Shao, W.Q. Jin, N.P. Xu, J.M. Ahn, *J. Power Sources* 180 (2008) 15–22.
- [4] E. Fabbri, S. Licoccia, E. Traversa, E.D. Wachsman, *Fuel Cells* 9 (2009) 128–138.
- [5] A. Grimaud, F. Mauvy, J.M. Bassat, S. Fourcade, L. Rocheron, M. Marrony, J.C. Grenier, *J. Electrochem. Soc.* 159 (2012) B683–B694.
- [6] J. Fleig, H.R. Kim, J. Jamnik, J. Maier, *Fuel Cells* 8 (2008) 330–337.
- [7] F.S. Baumann, J. Fleig, H.U. Habermeier, J. Maier, *Solid State Ionics* 177 (2006) 1071–1081.
- [8] L. Wang, R. Merkle, J. Maier, *J. Electrochem. Soc.* 157 (2010) B1802–B1808.
- [9] K.D. Kreuer, *Solid State Ionics* 125 (1999) 285–302.
- [10] T. Schöber, H.G. Bohn, *Solid State Ionics* 127 (2000) 351–360.
- [11] K.D. Kreuer, *Annu. Rev. Mater. Res.* 33 (2003) 333–359.
- [12] C. Kjolseth, H. Fjeld, O. Prytz, P.I. Dahl, C. Estournes, R. Haugsrud, T. Norby, *Solid State Ionics* 181 (2010) 268–275.
- [13] F. Iguchi, C.T. Chen, H. Yugami, S. Kim, *J. Mater. Chem.* 21 (2011) 16517–16523.
- [14] M. Shirpour, R. Merkle, C.T. Lin, J. Maier, *Phys. Chem. Chem. Phys.* 14 (2012) 730–740.
- [15] P. Babilo, T. Uda, S.M. Haile, *J. Mater. Res.* 22 (2007) 1322–1330.
- [16] F. Iguchi, T. Tsurui, N. Sata, Y. Nagao, H. Yugami, *Solid State Ionics* 180 (2009) 563–568.
- [17] M. Shirpour, B. Rahmati, W. Sigle, P.A. van Aken, R. Merkle, J. Maier, *J. Phys. Chem. C* 116 (2012) 2453–2461.
- [18] K. Nomura, H. Kageyama, *Solid State Ionics* 178 (2007) 661–665.
- [19] A. Grimaud, J.M. Bassat, F. Mauvy, P. Simon, A. Canizares, B. Rousseau, M. Marrony, J.C. Grenier, *Solid State Ionics* 191 (2011) 24–31.
- [20] W. Lai, S.M. Haile, *J. Am. Ceram. Soc.* 88 (2005) 2979–2997.
- [21] W. Lai, S.M. Haile, *Phys. Chem. Chem. Phys.* 10 (2008) 865–883.
- [22] K.L. Scholl, E.A. Fletcher, *Energy* 18 (1993) 69–74.
- [23] J. Jamnik, J. Maier, *Phys. Chem. Chem. Phys.* 3 (2001) 1668–1678.
- [24] K.D. Kreuer, S. Adams, W. Munch, A. Fuchs, U. Klock, J. Maier, *Solid State Ionics* 145 (2001) 295–306.
- [25] M. Oishi, S. Akoshima, K. Yashiro, K. Sato, J. Mizusaki, T. Kawada, *Solid State Ionics* 180 (2009) 127–131.
- [26] J. Fleig, *Solid State Ionics* 161 (2003) 279–289.
- [27] F.S. Baumann, J. Fleig, G. Cristiani, B. Stuhlhofer, H.U. Habermeier, J. Maier, *J. Electrochem. Soc.* 154 (2007) B931–B941.
- [28] M. Shirpour, R. Merkle, J. Maier, *Solid State Ionics* 216 (2012) 1–5.
- [29] J. Fleig, *Phys. Chem. Chem. Phys.* 7 (2005) 2027–2037.
- [30] J.H. Joo, R. Merkle, J. Maier, *J. Power Sources* 196 (2011) 7495–7499.
- [31] J.H. Joo, R. Merkle, J.H. Kim, J. Maier, *Adv. Mater.* 24 (2012) 6507–6512.
- [32] B.A. Boukamp, *priv. commun.* (2012).